20
Modeling Shearing of γ' in Ni-Based Superalloys

C. Shen, J. Li, M.J. Mills, and Y. Wang

Abstract

The activation energies associated with the formation of a superlattice intrinsic stacking fault (SISF) from an antiphase domain boundary (APB) and the formation of a superlattice extrinsic stacking fault (SESF) from a complex stacking fault (CSF) in γ' phase of Ni-based superalloys are calculated using a microscopic phase field dislocation model in combination with the nudged elastic band (NEB) method. The model incorporates the generalized stacking fault (GSF) energy and hence allows for dislocation dissociations. The results suggest that formation of SESF from CSF rather than formation of SISF from APB is most likely the operating mechanism for the isolated faulting of γ' precipitates observed in the experiments.

20.1
Introduction

In precipitation-hardened alloys, dislocation–precipitate interactions include Orowan looping, precipitate shearing, and dislocation climbing over the precipitates. In Ni-based superalloys all these mechanisms have been observed under different deformation or microstructural conditions [1–3]. The transition in deformation mode depends on precipitate size, applied stress, deformation temperature, and time at temperature (due to microstructural coarsening). The classic strengthening mechanism for Ni-based superalloys has been the shearing of γ' precipitates by pairs of $a/2\langle 110\rangle$ matrix dislocations coupled by an antiphase domain boundary (APB). Recent experimental observations [4], however, have shown that stacking faults rather than APBs are created in the γ' precipitates during deformation. Some of the possible mechanisms producing either a superlattice intrinsic stacking fault (SISF) or a superlattice extrinsic stacking fault (SESF) rather than an APB in the γ' phase have been proposed, including Kear [5] and Condat [6]. However, no quantitative calculations of the kinetics of these mechanisms exist.

Integral Materials Modeling: Towards Physics-Based Through-Process Models
Edited by Günter Gottstein

ISBN: 978-3-527-31711-0

Recently the energetics for the formation of SISF and SESF in γ' particles have been investigated using a quantitative microscopic-level phase field dislocation model [7]. In the present contribution the major features of the model and the main results on the activation energies for the formation of these two types of stacking fault are summarized. The results may shed light on the possible mechanisms of γ' shearing and microstructure sensitivity observed in disk alloys during their creep deformation.

20.2 Method

A dislocation can be considered as, instead of a singular defect line, a boundary that divides a glide plane into two areas that differ in inelastic shear displacement. The phase field models for dislocation glide [8, 9] utilize a field description of the inelastic shear displacement for dislocations. Although the inelastic displacement field is generally defined in a three-dimensional (3D) crystal, it is mostly concentrated in glide planes for dislocations and becomes nearly zero in magnitude in the remaining "good" crystal. In the glide plane, the inelastic displacement field varies rapidly only near the dislocation, by which the dislocation core is identified. The use of inelastic displacement or, more generally, the localized transformation strain field simplifies the description of dislocation in several aspects. Since dislocations are merely identified at the positions where the shear displacement changes rapidly on glide planes, the use of inelastic displacement field can naturally treat dislocations of arbitrary number and geometry in a 3D crystal. Introduction of the generalized stacking fault (GSF) energy to the phase field dislocation model [9, 10] allows the system to sample not only the "good" crystal and the dislocations, but also various stacking faults associated with dislocation activities. For example the creation and annihilation of APBs in γ' due to $a/2\langle 110\rangle$ γ-matrix dislocations has been simulated with no *ad hoc* treatment for the stacking faults [11].

20.2.1 Dislocation and Stacking Fault Modeling

Recently a microscopic-level phase field dislocation model was developed to study quantitatively dislocation core structures and various stacking faults [7]. The model uses the inelastic shear displacement field, $\mathbf{u}(\mathbf{r})$, to describe dislocations and stacking faults. The equilibrium state, as well as the dynamic evolution, of dislocations is governed by minimization of a total energy functional

$$E^{total}[\mathbf{u}(\mathbf{r})] = E^{cryst}[\mathbf{u}(\mathbf{r})] + E^{elast}[\mathbf{u}(\mathbf{r})] + W[\mathbf{u}(\mathbf{r})] \tag{20.1}$$

that consists of E^{cryst}, the crystalline energy, E^{elast}, the elastic energy, and W, the mechanical work by external loading. The crystalline energy (known as misfit en-

ergy in Peierls models [12, 13]) is a spatial integral of a nonconvex local density function that characterizes the interplanar misfit potential between the crystal halves at the two sides of the glide plane

$$E^{cryst} = \int \mathrm{d}\mathbf{r} \frac{\gamma(\mathbf{u}(\mathbf{r}))}{d} \tag{20.2}$$

where γ is the GSF energy and d the interplanar distance. The elastic energy, E^{elast}, based on 3D linear elasticity Green's function solution, is given in a close form in Fourier space as [14]

$$E^{elast} = \frac{1}{2}\int \frac{\mathrm{d}\mathbf{g}}{(2\pi)^3}[C_{ijkl}\tilde{\varepsilon}_{ij}(\mathbf{g})\tilde{\varepsilon}_{kl}(\mathbf{g}) - g_i\tilde{\sigma}_{ij}(\mathbf{g})\Omega_{jk}\tilde{\sigma}_{kl}(\mathbf{g})g_l/g^2] \tag{20.3}$$

where $\mathbf{g}$ is the reciprocal space vector, $\tilde{\varepsilon}_{ij}(\mathbf{g})$ is a Fourier transform of the inelastic (transformation) strain tensor $\varepsilon_{ij}(\mathbf{u}(\mathbf{r})) \equiv \mathbf{u}(\mathbf{r}) \otimes \mathbf{n}/d$, with $\mathbf{n}$ being the glide plane normal. $\tilde{\sigma}_{ij}(\mathbf{g}) \equiv C_{ijkl}\tilde{\varepsilon}_{kl}(\mathbf{g})$, $[\mathbf{\Omega}^{-1}]_{jk} = g_i g_l C_{ijkl}/g^2$, and C_{ijkl} is the elastic modulus tensor. The integral, converted to a discrete sum, is taken in the entire Brillouin zone except for a volume element of $(2\pi)^3/V$ at $\mathbf{g} = 0$, with V being the volume of the crystal. The mechanical work under applied stress σ_{ij}^{appl} is given by

$$W = \int \mathrm{d}\mathbf{r}\sigma_{ij}^{appl}(\mathbf{r})\varepsilon_{ij}(\mathbf{u}(\mathbf{r})) \tag{20.4}$$

Whereas the traditional gradient energy is absent in the model, the balance between the elastic energy and the crystalline energy naturally gives rise to a diffuse dislocation core at the length scale of Burgers vector. Additionally, relaxation of the inelastic shear displacement field is allowed only within the glide plane, which is the same as in the Peierls dislocation model [12, 13]. However, the phase field model offers the ability of treating arbitrary dislocation configurations. It enables an efficient computation of planar dislocation structures and stacking faults over a large length scale while maintaining a quantitative treatment of dislocation cores [7].

20.2.2
Calculation of Activation Energy

The APB and complex stacking fault (CSF) energies are much higher than that of the SISF and SESF in the γ' phase. However, the formation of SISF or SESF involves the creation of a new $a/6\langle 112\rangle$ dislocation loop. The change in the total energy may also include the interaction energy of the stacking fault with neighboring dislocations and the applied mechanical work, which are all included in Eq. (20.1). The minimum energy pathway and the corresponding activation energy can then be determined by locating the corresponding saddle point on the total energy surface.

An intuitive way is to sample the total energy surface by a series of trial stacking faults with predefined size and geometry. If the "planned" configurations are sufficiently close to that along the actual minimum energy path (MEP) of the fault formation, the total energy mapped out will initially increase with the area of the stacking fault and decrease afterwards, where the saddle point gives the activation energy. Furthermore, relaxation of each configuration via Ginzburg–Landau equation

$$\frac{\partial \mathbf{u}(\mathbf{r})}{\partial \tau} = -\frac{\delta E^{total}}{\delta \mathbf{u}(\mathbf{r})} \tag{20.5}$$

allows producing a more realistic relaxed dislocation core structure, and thus predicts more accurately the activation energy. This approach is used to study the formation of SISF. In Eq. (20.5) τ is the reduced time.

A more rigorous approach is to use the nudged elastic band (NEB) method [15–18], which is now widely applied in theoretical chemistry and condensed matter physics in finding MEP and saddle point on a high dimensional potential energy surface. With the phase field total energy functional (Eq. 20.1) the NEB method can be applied to identify the critical configuration and activation energy of the stacking fault without pre-assumption of its geometry. An example of using this approach to study the formation of SESF is also included.

20.3 Results

20.3.1 Nucleation of SISF from APB

Figure 20.1 shows the GSF energy for γ' phase on a (111) plane and various stacking faults with their associated Burgers vectors. The GSF energy is expressed in a 2D Fourier series on a (111) crystallographic plane with the base vectors being on the reciprocal lattice of the crystal [19], which naturally preserves the crystal symmetry. The Fourier series is fitted to the fault energies: $\gamma_{\mathrm{CSF}} = 221$ mJ/m^2, $\gamma_{\mathrm{SISF}} = 12.0$ mJ/m^2, and $\gamma_{\mathrm{APB}} = 172$ mJ/m^2. The elastic moduli used are $C_{11} = 224.3$ GPa, $C_{12} = 148.6$ GPa, $C_{44} = 125.8$ GPa [20].

The calculation of the activation energy of homogeneous nucleation of an SISF is performed in a cubic computational cell of edge length 200 nm, with periodic boundary conditions applied in all three dimensions. A circular $a/6\langle 112\rangle$ dislocation loop is placed on a prerelaxed APB (of which the shear displacement is automatically determined by the GSF energy) that extends throughout the entire simulation cell on a (111) glide plane. The system size is found sufficiently large that the effect from image dislocations is negligible. Each calculation uses a different radius for the loop, and the initial core profile of the dislocation is single-step sharp. The dislocation core is also relaxed with Eq. (20.5) for a certain number of

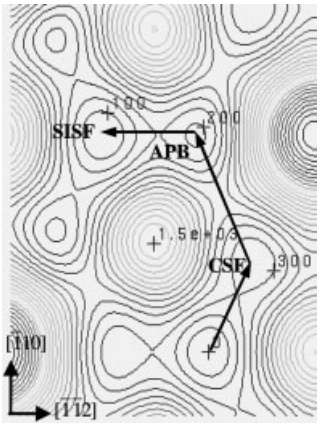

Fig. 20.1 GSF energy (in mJ m^{-2}) of Ni3Al for (111) plane.

iterations that have been found to be sufficient by a separate test on straight dislocations. The total energy of the system is then calculated using Eq. (20.1) for both unrelaxed and relaxed cases, and the results are plotted with respect to the loop radius in Fig. 20.2. In the plot the total energy is shifted by a reference energy of a configuration with pure APB. The activation energies are found to be 27.7 and 17.0 eV with and without core relaxation, respectively.

A more realistic configuration is illustrated in Fig. 20.3, where nucleation of an SISF is considered in a finite APB region with an additional interaction with the

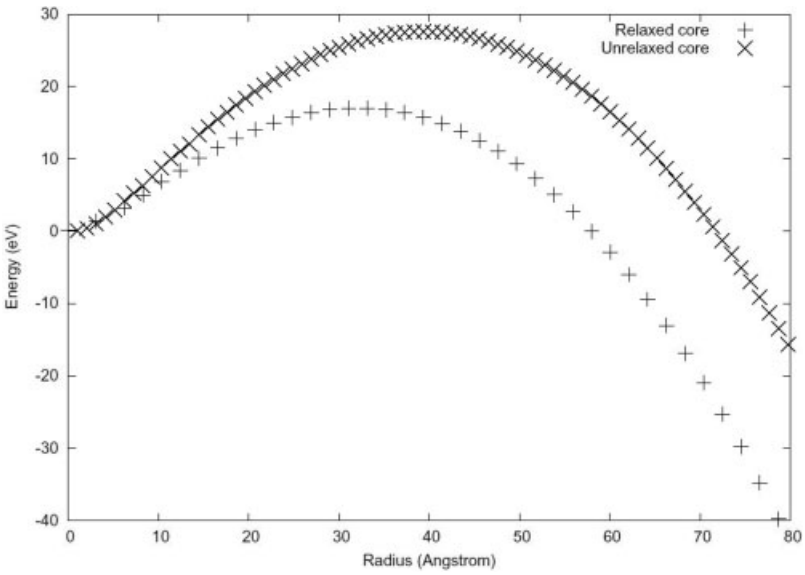

Fig. 20.2 Activation energy of homogeneous nucleation of SISF from APB.

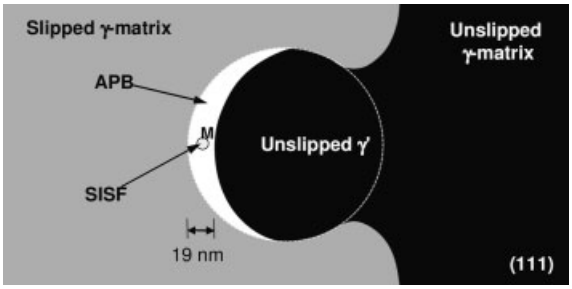

Fig. 20.3 Nucleation of SISF in a finite APB (at the marker M). Slip regions are shown in different shade. The γ' particle is outlined by the dashed circle.

leading $a/2\langle 110\rangle$ matrix dislocation. The simulation size is $424 \times 212 \times 212$ nm^3. The radius of the γ' particle and the interparticle spacing (due to the periodic boundary condition) are 140 and 72 nm, as provided from experimental observation. The initial configuration is produced by applying a resolved shear stress of 693 MPa on the matrix dislocation. The dislocation is forced through the γ matrix between two γ' particles, while in the meantime it partially cuts into the γ' particle. The configuration is found nearly in equilibrium under the applied stress. Afterwards a circular SISF is introduced in the same way as before. The activation energies are found to be respectively 22.7 and 17.7 eV with and without core relaxation (Fig. 20.4).

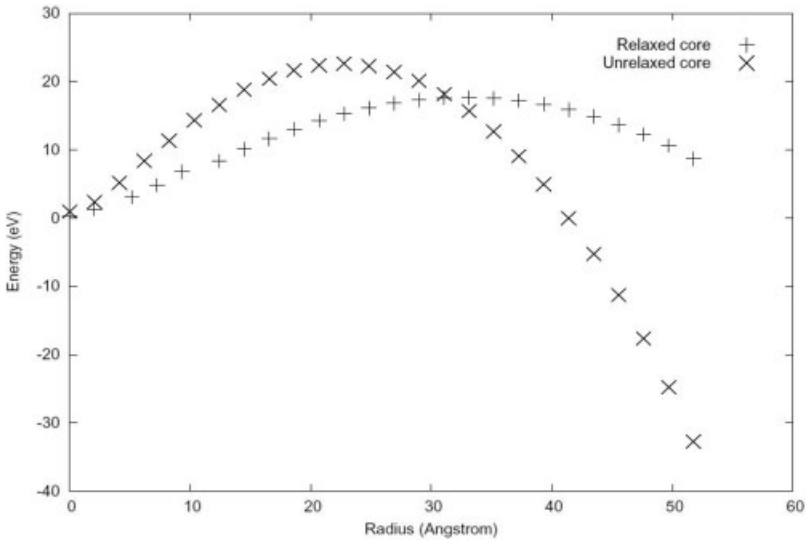

Fig. 20.4 Activation energy of nucleation of SISF in finite APB.

20.3.2
Nucleation of SESF from CSF

The calculated activation energies for the formation of SISF on APB seem too high for the process to be a plausible mechanism. Therefore, we consider the formation of SESF by successive $a/6\langle 112\rangle$ slip in two adjacent (111) glide planes and a subsequent short-range diffusive reordering between the two atomic planes [21]. Furthermore, we assume that the slip in one plane occurs much later than the slip in the other plane, so that the formation of SESF is equivalent to a homogeneous nucleation in the plane one atomic step above an existing infinite CSF. The second assumption may be considered reasonable since the repulsive force between the two identical $a/6\langle 112\rangle$ dislocations, if the leading one is still in the neighborhood, will considerably raise the barrier for SESF formation. The GSF energy in this case involves a two-layer configuration. Prior to a full planar potential being available, we use a GSF energy that is constrained along the $\langle 112\rangle$ direction, as shown in Fig. 20.5. The portion of the energy from CSF to pseudo twin corresponds to a slip on the second plane. At this moment the energy is simply rescaled to match the pseudo twin energy to the known SESF energy that accounts for the short-range reordering. A more accurate calculation is underway.

The system size considered for the calculation is 200 nm × 200 nm × 200 nm. Fifty images are used with the NEB calculation for the MEP and the activation energy. The two ending images correspond to an infinite CSF and an infinite SESF, respectively. All the remaining images are initially created by linear interpolation. We also applied an external stress along the $\langle 112\rangle$ direction with various magnitude to assist nucleation. Figure 20.6 shows the energies under an applied stress of 500 MPa. Since the geometry of the critical configuration is no

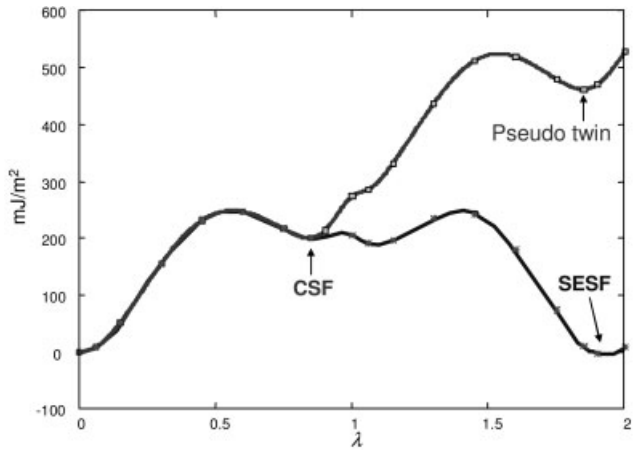

Fig. 20.5 Ni_3Al pseudo twinning multiplane generalized stacking fault energy (along $1/6\langle 112\rangle$) and the rescaled portion (approximately from $\lambda = 1$ to 2) for SESF after short-range reordering. The energy is calculated in VASP with 108 atoms.

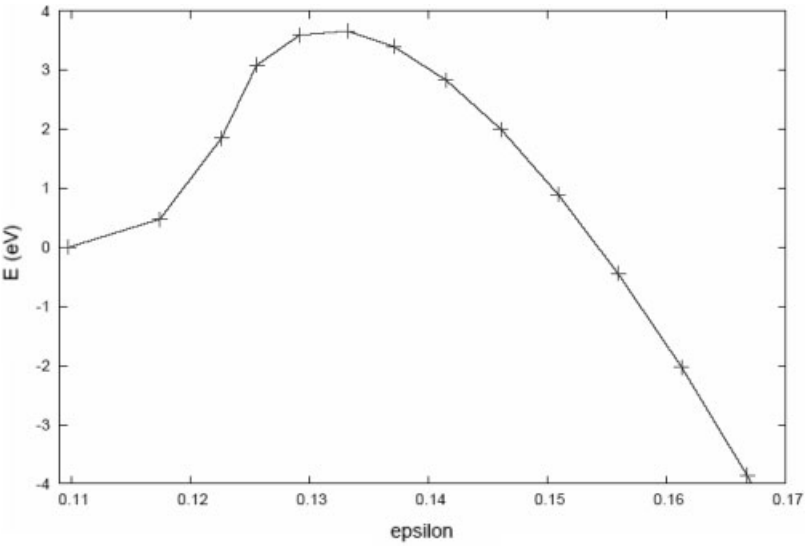

Fig. 20.6 Activation energy of formation of SESF from an infinite CSF.

longer an assigned parameter, we use the total inelastic strain in the glide plane as the indication of the size of the SESF nucleus. The activation energy is found to be 3.7 eV (Fig. 20.6). Moreover, as the applied stress increases to 600 MPa the activation energy reduces to 0.5 eV (Fig. 20.7).

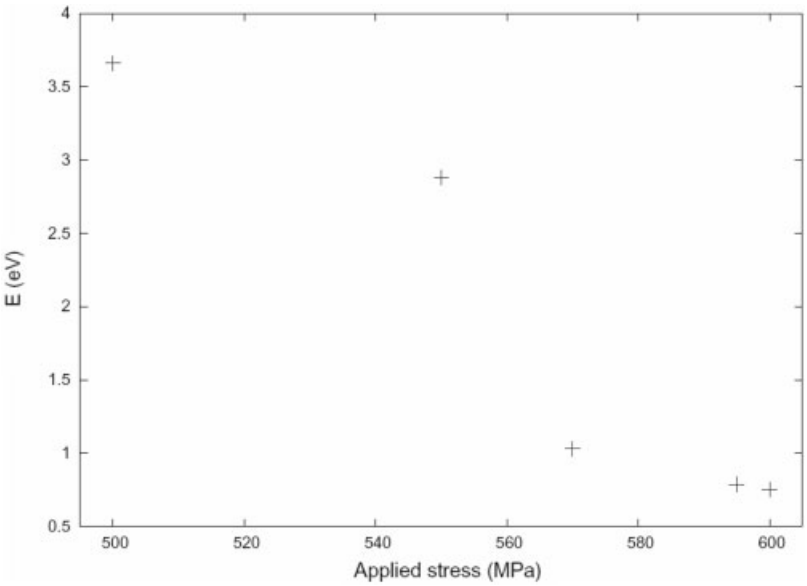

Fig. 20.7 Variation of the activation energy of SESF with applied stress.

20.4 Summary

Activation energies for nucleation of SESF in CSF and nucleation of SISF in APB are calculated using a microscopic phase field dislocation model combined with the NEB method. The results show that the activation energy for formation of an SESF is considerably lower than that for the formation of an SISF. Presence of dislocations in the neighborhood may alter the nucleation barrier. In the case of an SESF, since the leading $a/6\langle 112\rangle$ partial dislocation that creates the first layer CSF has the same Burgers vector as the dislocation that subsequently produces the SESF, their mutual repulsive elastic interaction is expected to increase the activation energy. In the case of SISF, however, the Burgers vector of the leading $a/2\langle 110\rangle$ matrix dislocation is nearly perpendicular to the one that connects APB to SISF. Their elastic interaction has little effect on the activation energy, as indicated by the calculation. Under an applied stress the activation energy for SESF can be reduced considerably, e.g., from 3.7 eV at 500 MPa to 0.5 eV at 600 MPa. Since the two partial dislocations in the two layers of CSF have the same Burgers vector, the optimal stress direction is parallel to the Burgers vector, because it can facilitate the formation of both CSF and SESF. For SISF, since the two Burgers vectors are normal to each other, the effect of the applied stress is reduced. With a rough estimate, the activation energy with an applied stress in the direction 45° to both Burgers vectors (with no relaxation of dislocation core) can be reduced by 30%.

Acknowledgments

This work is supported by US Air Force Office of Scientific Research through the MEANS2 program (Grant No. FA9550-05-1-0135) and by the Office of Naval Research through the D3D program (Grant No. N00014-05-1-0504).

References

1 D. Mukherji, F. Jiao, W. Chen, R. P. Wahi, *Acta Metall. Mater.* 39, 1991, 1515.
2 Y. H. Zhang, Q. Z. Chen, D. M. Knowles, *Mater. Sci. Technol.* 17, 2001, 1551.
3 B. Decamps, S. Raujol, A. Coujou, F. Pettinari-Sturmel, N. Clement, D. Locq, P. Caron, *Phil. Mag.* 84, 2004, 91.
4 G. B. Viswanathan, P. M. Sarosi, M. F. Henry, D. D. Whitis, W. W. Milligan, M. J. Mills. *Acta Mater.* 53, 2005, 3041.
5 B. H. Kear, J. M. Oblak, A. F. Giamei, *Metall. Trans.* 1, 1970, 2477.
6 M. Condat, B. Décamps, *Scripta Metall.* 21, 1987, 607.
7 C. Shen, J. Li, Y. Wang, manuscript in preparation.
8 Y. U. Wang, Y. M. Jin, A. M. Cuitino, A. G. Khachaturyan, *Acta Mater.* 49, 2001, 1847.
9 C. Shen, Y. Wang, *Acta Mater.* 51, 2003, 2595.
10 C. Shen, Y. Wang, *Acta Mater.* 52, 2004, 683.

11 C. Shen, M. J. Mills, Y. Wang. *Mater. Res. Soc. Symp. Proc.*, 753, 2002, BB5.21.21.

12 R. E. Peierls, *Proc. Phys. Soc.* 52, 1940, 23.

13 F. R. N. Nabarro, *Proc. Phys. Soc.* 59, 1947, 256.

14 A. G. Khachaturyan, *Theory of Structural Transformations in Solids*, John Wiley, New York, 1983.

15 G. Mills, H. Jonsson, *Phys. Rev. Lett.* 72, 1994, 1124.

16 G. Mills, H. Jonsson, G. K. Schenter, *Surf. Sci.* 324, 1995, 305.

17 H. Jonsson, G. Mills, K. W. Jacobsen, in *Classical and Quantum Dynamics in Condensed Phase Simulations*, ed. B. J. Berne, G. Ciccotti, D. F. Coker, World Scientific 1998, p. 385.

18 G. Henkelman, H. Jonsson, *J. Chem. Phys.* 113, 2000, 9978.

19 G. Schoeck (private communication).

20 F. Kayser, C. Stassis. *Phys. Stat.* 64, 1981, 335.

21 M. Kolbe, *Mater. Sci. Eng. A* 319, 2001, 383.